THE ASTROPHYSICAL JOURNAL, 558:29–41, 2001 September 1
© 2001. The American Astronomical Society. All rights reserved. Printed in U.S.A.

LENSING-INDUCED NON-GAUSSIAN SIGNATURES IN THE COSMIC MICROWAVE BACKGROUND

MASAHIRO TAKADA
Division of Theoretical Astrophysics, National Astronomical Observatory, 2-21-1 Osawa, Mitaka, Tokyo 181-8588, Japan; mtakada@th.nao.ac.jp
Received 2000 November 12; accepted 2001 May 4

ABSTRACT

We propose a new method for extracting non-Gaussian signatures on isotemperature statistics in the cosmic microwave background (CMB) sky, which are induced by the gravitational lensing due to the intervening large-scale structure of the universe. To develop the method, we focus on a specific statistical property of the intrinsic Gaussian CMB field: a field point in the map that has a larger absolute value of the temperature threshold tends to have a larger absolute value of the curvature parameter defined by a trace of the second-derivative matrix of the temperature field, while the ellipticity parameter similarly defined is uniformly distributed independently of the threshold because of the isotropic nature of the Gaussian field. Weak lensing then causes a stronger distortion effect on the isotemperature contours with higher thresholds and especially induces a coherent distribution of the ellipticity parameter correlated with the threshold as a result of the coupling between the CMB curvature parameter and the gravitational tidal shear in the observed map. These characteristic patterns can be statistically picked up by considering three independent characteristic functions, which are obtained from the averages of quadratic combinations of the second-derivative fields of the CMB over isotemperature contours with each threshold. Consequently, we find that the lensing effect generates non-Gaussian signatures on those functions that have a distinct functional dependence on the threshold. We test the method using numerical simulations of CMB maps and show that the lensing signals can be measured definitely, provided that we use CMB data with sufficiently low noise and high angular resolution.

Subject headings: cosmic microwave background — cosmology: theory — gravitational lensing — large-scale structure of universe

1. INTRODUCTION

Determination of the power spectrum of dark matter fluctuations in the observed hierarchical large-scale structures of the universe remains perhaps the compelling problem in cosmology. Weak gravitational lensing due to large-scale structure is recognized as a powerful probe for solving this problem as well as for constraining the cosmological parameters (Gunn 1967; Blandford et al. 1991; Miralda-Escude 1991; Kaiser 1992), because it can fully avoid uncertainties associated with the biasing problem. Recently, several independent groups have reported significant detections of coherent gravitational distortions of distant galactic images (Van Waerbeke et al. 2000b; Wittman et al. 2000; Bacon, Refregier, & Ellis 2000; Kaiser, Wilson, & Luppino 2000; Maoli et al. 2001). On the other hand, the temperature anisotropies in the cosmic microwave background (CMB) can be the most powerful probe of our universe, especially of fundamental cosmological parameters (e.g., Hu, Sugiyama, & Silk 1997). Weak lensing similarly induces distortions in the pattern of CMB anisotropies, and lensing signatures will provide a wealth of information on inhomogeneous matter distribution and the evolutionary history of dark matter fluctuations between the last scattering surface and the present. We thus expect that the cosmological implications provided from the measurements of lensing effects on the CMB will be very precise, because there is no ambiguity in the theoretical understanding of the primary CMB physics and about the distance of the source plane. However, it is concluded that weak-lensing effects on the CMB angular power spectrum C_l are small (e.g., see Seljak 1996 and references therein), although detailed CMB analyses need to also take into account the lensing contribution. Recently, Seljak & Zaldarriaga (1999; see also Zaldarriaga & Seljak 1999) developed a new method for a direct reconstruction of the projected matter power spectrum from the observed CMB map and showed that it could be successfully achieved if there is no sufficient small-scale power of intrinsic CMB anisotropies. In this method, the lensing signals can be extracted by averaging quadratic combinations of the CMB derivative fields over many independent CMB patches like the analysis to extract the distortion effect on distant galactic images, even though the reconstruction maps have a low signal-to-noise ratio on individual patches.

Excitingly, the high-precision data from BOOMERANG (de Bernardis et al. 2000; Lange et al. 2001) and MAXIMA-1 (Hanany et al. 2000; Balbi et al. 2000) have revealed that the measured angular power spectrum C_l is fairly consistent with that predicted by the inflation-motivated adiabatic cold dark matter models (also see Tegmark & Zaldarriaga 2000; Hu et al. 2001). The standard inflationary scenarios also predict that the primordial fluctuations are homogeneous and isotropically Gaussian (Guth & Pi 1982), and thus statistical properties of any CMB field can be completely determined from the two-point correlation function $C(\theta)$, or equivalently, C_l, based on Gaussian random theory (Bardeen et al. 1986, hereafter BBKS; Bond & Efstathiou 1987, hereafter BE). Taking advantage of this predictability, various statistical methods to extract the non-Gaussian signatures induced by weak lensing have been proposed. Bernardeau (1998) found that lensing alters a specific shape of the probability distribution function (PDF) of the ellipticity parameter for the field point or the peak for the Gaussian case as a result of an excess of elongated structures in the observed (lensed) map. Although the method could be a powerful probe to measure the matter fluctuations around the characteristic curvature scale of the CMB, the beam-smearing effect of a telescope is crucial for detection because

it again tends to circularize the deformed structures. Van Waerbeke, Bernardeau, & Benabed (2000a) then investigated that a statistically correlated alignment between the CMB and distant galactic ellipticities could be detected with a higher signal-to-noise ratio, provided that a galaxy survey follow-up can be done on a sufficiently large area. We have quantitatively investigated the weak-lensing effect on the two-point correlation function of local maxima or minima in the CMB map, and it can potentially probe the lensing signatures on large angular scales such as $\theta \approx 70'$, which corresponds to matter fluctuations with wavelength modes around $\lambda \sim 50\ h^{-1}$ Mpc (Takada, Komatsu, & Futamase 2000; Takada & Futamase 2001). Recently, using numerical simulations, it was shown that the lensing effect causes a change of normalization factors for three morphological descriptions of the CMB map, the so-called Minkowski functionals, against their Gaussian predictions (Schmalzing, Takada, & Futamase 2000).

The purpose of this paper is to develop a new simple method for extracting the lensing-induced non-Gaussian signatures from the CMB map based on the isotemperature statistics. We thus focus on specific statistical properties of the intrinsic Gaussian CMB field: a field point that has a larger absolute value of the temperature threshold tends to have a larger absolute value of the curvature parameter defined by a trace of the second-derivative matrix of the CMB field, while the ellipticity parameter similarly defined is uniformly distributed independently of the threshold because of the isotropic nature of the Gaussian field. From these features, we expect that weak lensing causes a larger distortion effect on structures of temperature fluctuations around a point with a higher threshold. In particular, lensing can induce a coherent distribution of the ellipticity parameter correlated with the threshold owing to the coupling between the CMB curvature and the gravitational tidal shear. To extract these characteristic patterns, we define three independent functions based on the isotemperature statistics that are obtained from the averages of quadratic combinations of the second derivatives of the CMB field over isotemperature contours with each threshold. As a result, we find that the lensing effect on those characteristic functions generates a definite functional dependence on the threshold, and therefore the lensing signals could be easily measured as a non-Gaussian signature since those functions have very specific shapes in the Gaussian (unlensed) case. Using numerical simulations of lensed and unlensed CMB maps including the instrumental effects of beam smearing and detector noise, we investigate the feasibility of this method.

This paper is organized as follows: In § 2 we formulate a method for extracting the lensing-induced non-Gaussian signatures using Gaussian random theory for the primary CMB. In § 3 we outline the procedure of numerical experiments of our method using simulated CMB maps with and without the weak-lensing effect. In § 4 we present some results in a flat universe with a cosmological constant and investigate the detectability of lensing signatures by taking into account the measurement errors associated with cosmic variance and instrumental effects, especially for the future satellite mission *Planck Surveyor*.[1] In the final section some discussions and conclusions are presented.

[1] See http://astro.estec.esa.nl/SA-general/Projects/Planck.

2. METHOD: WEAK-LENSING EFFECT ON ISOTEMPERATURE STATISTICS

2.1. *Random Gaussian Theory*

In this section, we briefly review a relevant part of the Gaussian random theory developed by BBKS and BE for three- and two-dimensional cases, respectively. First, we define the temperature fluctuation field in the CMB map as $\Delta(\boldsymbol{\theta}) \equiv [T(\boldsymbol{\theta}) - T_{\rm CMB}]/T_{\rm CMB}$. Throughout this paper we employ the flat sky approximation developed by BE, and this is a good approximation for our study because the lensing deformation effect on CMB anisotropies is important only on arcminute scales. The Fourier transformation can be then expressed as $\Delta(\boldsymbol{\theta}) \equiv \int d^2\boldsymbol{l}/(2\pi)^2 \Delta(\boldsymbol{l}) e^{i\boldsymbol{l}\cdot\boldsymbol{\theta}}$, and the statistical properties of the unlensed CMB are completely specified by the angular power spectrum C_l defined by $\langle \Delta(\boldsymbol{l})\Delta(\boldsymbol{l}')\rangle = (2\pi)^2 C_l \delta^2(\boldsymbol{l} - \boldsymbol{l}')$.

According to Gaussian random theory, a certain set of variables $v_i (i = 1, 2, \ldots, N)$ constructed from the CMB field obeys the following joint PDF:

$$p(\boldsymbol{v}) = \frac{1}{(2\pi)^{N/2} |\det (M_{ij})|} \exp\left(-\frac{1}{2} v_i M_{ij}^{-1} v_j\right), \quad (1)$$

where M_{ij} is the covariance matrix defined by $M_{ij} \equiv \langle (v_i - \langle v_i\rangle)(v_j - \langle v_j\rangle)\rangle$ and M^{-1} and $\det (M_{ij})$ denote the inverse and determinant, respectively. Since we are interested in the lensing distortion effect on the isotemperature contours as a function of the temperature threshold, we pay special attention to the statistical properties of the second-derivative field of Δ, because the local curvature of the CMB is probably a good indicator of the lensing distortion effect, as shown later. It is thus convenient to introduce the following variables:

$$\nu \equiv \frac{\Delta}{\sigma_0}, \; X \equiv -\frac{\Delta_{11} + \Delta_{22}}{\sigma_2}, \; Y \equiv \frac{\Delta_{11} - \Delta_{22}}{\sigma_2},$$

$$Z \equiv \frac{2\Delta_{12}}{\sigma_2}, \quad (2)$$

where σ_n is defined by $\sigma_n^2 \equiv \int (l\, dl/2\pi) C_l l^{2n}$, $\Delta_{ij} \equiv \partial^2\Delta/\partial\theta^i\partial\theta^j$, and ν is the so-called *threshold* of temperature fluctuations. To clarify the physical meanings of X, Y, and Z more explicitly, we express them in terms of two eigenvalues λ_1 and λ_2 for a normalized curvature matrix $-\Delta_{ij}/\sigma_2$ as

$$X = -(\lambda_1 + \lambda_2), \; Y = -2eX \cos(2\varphi),$$

$$Z = -2eX \sin(2\varphi), \quad (3)$$

where e represents the local ellipticity parameter defined by $e \equiv (\lambda_1 - \lambda_2)/[2(\lambda_1 + \lambda_2)]$ and φ denotes the relative angle between the principal axis of Δ_{ij} and the one axis. By the meaning of the above equation, hereafter we call X a local *curvature parameter* around a given field point. Moreover, if the isotemperature contour in the neighborhood of local minima or maxima is given by an ellipse of $f(\theta_1, \theta_2) = \theta_1^2/b^2 + \theta_2^2/a^2$ in the coordinates of the principal axes, the parameter e can be expressed in terms of a and b as $e = (a^2 - b^2)/[2(a^2 + b^2)]$. Hence, Y and Z represent one- and two-axis components, respectively, of the local ellipticity parameter of the temperature curvature field. The nonzero second moments of variables (2) can be then calculated as

$$\langle \nu^2\rangle = \langle X^2\rangle = 2\langle Y^2\rangle = 2\langle Z^2\rangle = 1, \; \langle \nu X\rangle = \gamma_*, \quad (4)$$

where $\gamma_* = \sigma_1^2/(\sigma_0\,\sigma_2)$ (although we will also use the same letter γ for a shear component of lensing deformation tensor, we want readers not to confuse γ_* and γ) and γ_* represents the strength of cross-correlation between X and ν from the relation of $\gamma_* = \langle \nu X \rangle$. Equation (1) tells us that the joint PDF of variables $v_i = (\nu, X, Y, Z)$ for one field point becomes

$$p(\nu, X, Y, Z) = \frac{2}{(2\pi)^2\sqrt{1-\gamma_*^2}} \exp\,(-Q)\,, \tag{5}$$

with

$$2Q \equiv \nu^2 + \frac{(X-\gamma_*\,\nu)^2}{(1-\gamma_*^2)^2} + 2Y^2 + 2Z^2\,. \tag{6}$$

The important result is that ν and X have a nonvanishing cross-correlation, and the term $\exp\,\{-(X-\gamma_*\,\nu)^2/[2(1-\gamma_*^2)]\}$ in equation (5) physically means that structures around a field point with a larger absolute threshold tend to have a larger absolute value of the curvature parameter X. In fact, this feature is more explicitly clarified by considering the conditional probability distribution for field points with a given threshold ν. Figure 1 shows the distribution of curvature parameter X subject to the constraint that the point has a given threshold ν, where the conditional PDF is defined by $p(X\,|\,\nu) \equiv p(\nu, X)/p(\nu) = 1/[2\pi(1-\gamma_*^2)]^{1/2}$ $\exp\,\{-(X-\gamma_*\,\nu)^2/[2(1-\gamma_*^2)]\}$. The absence of correlation between ν and Y or Z is the consequence of the isotropic nature of the Gaussian field, more specifically, due to the isotropic distribution of an orientation angle of the ellipticity parameter.

Using the PDF (5), we define the following three independent functions with respect to the temperature threshold ν_t that characterize statistical properties of second-derivative fields of the CMB along isotemperature contours with the threshold ν_t:

$$V_X(\nu_t) = \langle \delta(\nu-\nu_t) X^2 \rangle = \frac{1}{\sqrt{2\pi}} \exp\left(-\frac{\nu_t^2}{2}\right) \times\,[(1-\gamma_*^2) + \gamma_*^2\,\nu_t^2]\,,$$

$$V_Y(\nu_t) = \langle \delta(\nu-\nu_t) Y^2 \rangle = \frac{1}{2\sqrt{2\pi}} \exp\left(-\frac{\nu_t^2}{2}\right),$$

$$V_Z(\nu_t) = \langle \delta(\nu-\nu_t) Z^2 \rangle = V_Y(\nu_t)\,, \tag{7}$$

where the bracket is defined by $\langle \cdots \rangle \equiv \int d\nu\,dX\,dY\,dZ \cdots p(\nu, X, Y, Z)$ and can be observationally interpreted as the average of the considered local quantities performed over all the isocontours in the CMB sky from the assumption of large-scale statistical homogeneity. All other averages of quadratic combinations of the second derivatives such as $\langle XY \rangle = \langle XZ \rangle = \langle YZ \rangle$ vanish because of the isotropic nature of the Gaussian field. The functions in equation (7) thus have very specific shapes for the Gaussian case, and we can take advantage of this property in order to extract the non-Gaussian signatures on those functions induced by the lensing distortion effect.

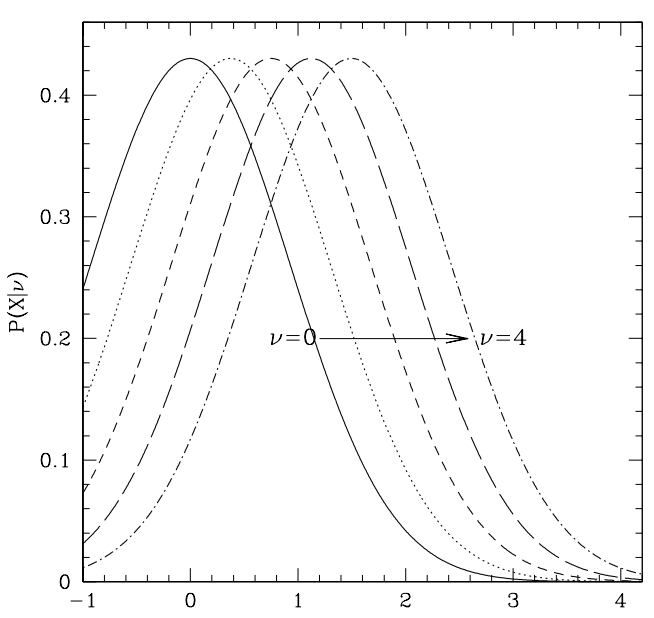

FIG. 1.—Conditional probability distributions of the curvature parameter X for a field point with height $\nu = 0$ (*solid curve*), $\nu = 1$ (*dotted curve*), $\nu = 2$ (*short-dashed curve*), $\nu = 3$ (*long-dashed curve*), and $\nu = 4$ (*dot-dashed curve*) are plotted for $\gamma_* = 0.35$.

2.2. *Lensing Distortion Effect on the Isotemperature Contours As a Non-Gaussian Signature*

The CMB photon rays are randomly deflected by the inhomogeneous matter distributions inherent in the intervening large-scale structures of the universe during their propagations from the last scattering surface to us. Therefore, the observed CMB temperature fluctuation field at a certain angular direction $\boldsymbol{\theta}$, $\tilde{\Delta}(\boldsymbol{\theta})$, is equal to the primary field emitted from the another direction $\boldsymbol{\theta} + \boldsymbol{\xi}(\boldsymbol{\theta})$ on the last scattering surface, $\Delta(\boldsymbol{\theta} + \boldsymbol{\xi})$, where $\boldsymbol{\xi}(\boldsymbol{\theta})$ is the displacement field. The lensed second-derivative field of the CMB can be then expressed by

$$\tilde{\Delta}_{ij} = (\delta_{im} + \xi_{m,i})\Delta_{mn}(\delta_{nj} + \xi_{n,j}) + \Delta_m\,\xi_{m,ij} = \mathcal{A}_{im}\,\Delta_{mn}\,\mathcal{A}_{nj} + \Delta_m\,\xi_{m,ij}\,, \tag{8}$$

where $\mathcal{A}$ is the so-called amplification matrix and δ_{ij} is the Kronecker delta symbol. Hereafter, the variables with and without the tilde symbol denote the lensed and unlensed CMB fields, respectively. The components of $\mathcal{A}_{ij}$ can be expressed in terms of the local gravitational convergence κ and tidal distortion γ as

$$\mathcal{A}_{ij} = \begin{pmatrix} 1-\kappa-\gamma_1 & -\gamma_2 \\ -\gamma_2 & 1-\kappa+\gamma_1 \end{pmatrix}. \tag{9}$$

In the weak-lensing regime the matrix $\mathcal{A}$ is always regular, and the variances of κ, γ_1, and γ_2 are related to each other through

$$\langle \kappa^2 \rangle = 2\langle \gamma_1^2 \rangle = 2\langle \gamma_2^2 \rangle = \sigma_\kappa^2\,. \tag{10}$$

We here have not assumed that κ and γ_i are Gaussian, and this is a simple consequence of statistical isotropy of the displacement field. As shown by the several works using the ray-tracing simulations through the large-scale structure modeled by N-body simulations, the lensing fields are indeed not Gaussian on angular scales of $\theta \lesssim 10'$ (Jain, Seljak, & White 2000; Hamana, Martel, & Futamase 2000),

and we will later discuss the problem of how the non-Gaussian features of κ could affect our results. The second moment of the convergence, σ_κ, is related to the projected matter power spectrum (Kaiser 1992):

$$\sigma_\kappa^2 = \int \frac{l\,dl}{2\pi} P_\kappa(l) = \frac{9}{4} H_0^4 \Omega_m^2 \int \frac{l\,dl}{2\pi} \times \int_0^{\chi_{\rm rec}} d\chi a^{-2}(\tau) W^2(\chi, \chi_{\rm rec}) P_\delta\left(k = \frac{l}{r(\chi)}, \chi\right), \quad (11)$$

where $P_\delta(k)$ and $P_\kappa(l)$ denote the three-dimensional power spectrum of matter fluctuations and its projected power spectrum, respectively. The term τ is a conformal time, $\chi \equiv \tau_0 - \tau$, and the subscripts 0 and "rec" denote values at present and the recombination time, respectively. H_0 ($=100\,h$ km s^{-1} Mpc^{-1}) and Ω_{m0} denote the present-day Hubble constant and energy density parameter of matter, respectively. The term $r(\chi)$ is the corresponding comoving angular diameter distance, defined as $K^{-1/2}\sin K^{1/2}\chi$, χ, and $(-K)^{-1/2}\sinh(-K)^{1/2}\chi$ for $K > 0$, $K = 0$, and $K < 0$, respectively, where the curvature parameter K is represented as $K = (\Omega_{m0} + \Omega_{\lambda 0} - 1)H_0^2$, and $\Omega_{\lambda 0}$ is the present-day vacuum energy density relative to the critical density. The projection operator $W(\chi, \chi_{\rm rec})$ on the celestial sphere is given by $W(\chi, \chi_{\rm rec}) = r(\chi_{\rm rec} - \chi)/r(\chi_{\rm rec})$. As shown later, the effect of the finite beam size $\theta_{\rm FWHM}$ of a telescope on σ_κ appears as a cutoff at $l \gtrsim l_{\rm sm}$ in the integration of equation (11) from the relation of $l_{\rm sm} \sim 1/\theta_{\rm FWHM}$, and thus σ_κ also depends on $\theta_{\rm FWHM}$ in a general case. Inversely, by changing the smoothing scale artificially, we could reconstruct the scale dependence of the projected matter power spectrum, and we will also investigate this possibility. The important result of equation (11) is that the magnitude of σ_κ is sensitive to Ω_{m0} and particularly to the normalization of the matter power spectrum of P_δ, which is conventionally expressed in terms of the rms mass fluctuations of a sphere of $8\,h^{-1}$ Mpc, i.e., σ_8. Similarly, variances of the second-derivative fields of displacement field ξ_i can be calculated as

$$\langle \xi_{1,11}^2 \rangle = 5\langle \xi_{1,12}^2 \rangle = 5\langle \xi_{1,11}\,\xi_{1,22} \rangle = 5\langle \xi_{1,12}\,\xi_{2,22} \rangle = \frac{5}{16} s^2 \quad (12)$$

with

$$s^2 \equiv 4\int \frac{l\,dl}{2\pi} l^4 P_\kappa(l)\,. \quad (13)$$

Equation (8) yields the following relations between the lensed (observed) and primary components of the second curvature matrix of temperature fluctuations up to the second order of ξ:

$$\tilde{X} = [(1-\kappa)^2 + \gamma^2]X + 2\gamma_1 Y + 2\gamma_2 Z - \frac{\Delta_i}{\sigma_2}(\xi_{i,11} + \xi_{i,22})\,,$$

$$\tilde{Y} = [(1-\kappa)^2 + \gamma_1^2 - \gamma_2^2]Y + 2\gamma_1 X + \frac{\Delta_i}{\sigma_2}(\xi_{i,11} - \xi_{i,22})\,,$$

$$\tilde{Z} = [(1-\kappa)^2 - \gamma_1^2 + \gamma_2^2]Z + 2\gamma_2 X + \frac{\Delta_i}{\sigma_2}\xi_{i,12}\,, \quad (14)$$

where we have ignored the second-order contributions of $\kappa\gamma_i$, $\gamma_1\gamma_2$, and so on because they vanish after the average as a consequence of the statistical isotropy of ξ_i. Note that weak lensing does not change the relations between second moments of these lensed variables compared with the Gaussian cases (4); $\langle \tilde{X}^2 \rangle = 2\langle \tilde{Y}^2 \rangle = 2\langle \tilde{Z}^2 \rangle \approx 1 + 10\sigma_\kappa^2$. Equation (14) for $\tilde{Y}$ or $\tilde{Z}$ implies that the lensing effect could induce an ellipticity parameter at a certain field point that arises from a coupling between the curvature parameter X and the gravitational shear γ even if the intrinsic ellipticity is zero ($Y = Z = 0$). Since this effect is observable only in a statistical sense, we focus our investigations on the problem of how the lensing alters statistical properties of the CMB second-derivative fields based on the isotemperature statistics.

Now we present theoretical predictions of lensed functions (7) with respect to the temperature threshold in the observed CMB map. If we assume that the primary CMB fields on the last scattering surface and the lensing displacement field due to large-scale structure are statistically independent, after straightforward calculations we can obtain

$$\tilde{V}_X(\nu_t) = \langle \delta(\tilde{\nu} - \nu_t)\tilde{X}^2 \rangle = \frac{1}{\sqrt{2\pi}} \exp\left(-\frac{\nu_t^2}{2}\right) \times \left\{(1 + 8\sigma_\kappa^2)[(1-\gamma_*^2) + \gamma_*^2 \nu_t^2] + 2\sigma_\kappa^2 + \frac{\sigma_1^2}{2\sigma_2^2} s^2\right\},$$

$$\tilde{V}_Y(\nu_t) = \langle \delta(\tilde{\nu} - \nu_t)\tilde{Y}^2 \rangle = \frac{1}{2\sqrt{2\pi}} \exp\left(-\frac{\nu_t^2}{2}\right) \times \left\{(1 + 6\sigma_\kappa^2) + 4\sigma_\kappa^2[(1-\gamma_*^2) + \gamma_*^2 \nu_t^2] + \frac{\sigma_1^2}{4\sigma_2^2} s^2\right\},$$

$$\tilde{V}_Z(\nu_t) = \tilde{V}_Y(\nu_t)\,. \quad (15)$$

We so far have used the perturbations only for the lensing displacement field ξ, and thus these equations (15) are valid for an arbitrary threshold ν_t. Equation (15) clearly shows that one of the lensing effects on these functions is the change of their normalization factors. Another important effect is that the lensing generates a characteristic functional dependence on ν_t of $V_X(\nu_t)$, $V_Y(\nu_t)$, and $V_Z(\nu_t)$. This is as a consequence of the coupling between the CMB curvature X and the gravitational tidal shear γ through the intrinsic correlation between ν_t and X and physically means that the lensing effect distorts more strongly the isotemperature contours that have a larger absolute threshold.

In practice it will be rather difficult to discriminate the change of normalization factors caused by lensing in equation (15) from the Gaussian case, because measurements of the normalizations in the CMB map might also be sensitive to systematic errors due to, for example, the discrete pixel effect in the map. For this reason, we here focus on the non-Gaussian signatures that have a distinct functional dependence on ν_t and consider the following observable functions normalized by their values at $\nu_t = 0$ as a deviation

from the specific function $\exp[-\nu_t^2/2]$:

$$F_X(\nu_t) \equiv \frac{\tilde{V}_X(\nu_t)}{\tilde{V}_X(0)} - \exp\left(-\frac{\nu_t^2}{2}\right) \approx \exp\left(-\frac{\nu_t^2}{2}\right) \frac{(1+8\sigma_\kappa^2)\gamma_*^2\,\nu_t^2}{1-\gamma_*^2+10\sigma_\kappa^2-8\sigma_\kappa^2\gamma_*^2},$$

$$F_Y(\nu_t) \equiv \frac{\tilde{V}_Y(\nu_t)}{\tilde{V}_Y(0)} - \exp\left(-\frac{\nu_t^2}{2}\right) \approx \exp\left(-\frac{\nu_t^2}{2}\right) \frac{4\sigma_\kappa^2\gamma_*^2\,\nu_t^2}{1+10\sigma_\kappa^2-4\sigma_\kappa^2\gamma_*^2},$$

$$F_Z(\nu_t) \equiv \frac{\tilde{V}_Z(\nu_t)}{\tilde{V}_Z(0)} - \exp\left(-\frac{\nu_t^2}{2}\right) = F_Y(\nu_t)\,, \tag{16}$$

where we have neglected the terms including contributions of s^2 in equation (15) because we numerically confirmed that the contributions are always small. In the following discussions, these three independent functions (16) are compared to the results of numerical experiments. Most importantly, equation (16) shows that, although for the Gaussian case in the absence of lensing we should have $F_Y(\nu_t) = F_Z(\nu_t) = 0$ for all ν_t because of $\sigma_\kappa = 0$, weak lensing induces distinct non-Gaussian signatures expressed as $\propto \nu_t^2\gamma_*^2 \exp(-\nu_t^2/2)$. Therefore, those two functions can be direct measures of the lensing distortion effect on the isotemperature contours. The property of $F_Y(\nu_t) = F_Z(\nu_t)$ arises from the statistical random orientations of both the CMB ellipticity parameter and the gravitational tidal shear, and we can use the relation to distinguish or check the lensing signals against other possible secondary non-Gaussian contributions. The lensing effects on F_X, F_Y, and F_Z depend on the two parameters γ_* and σ_κ. Then, note that γ_* is a *parameter* of the primordial CMB anisotropy field, which is not observable, and is related to the corresponding direct observable quantity $\tilde{\gamma}_*$ in the lensed CMB map by $\tilde{\gamma}_* \approx \gamma_*(1 - 7\sigma_\kappa^2/2)$, where $\tilde{\gamma}_*$ is defined by $\tilde{\gamma}_* = \tilde{\sigma}_1^2/(\tilde{\sigma}_0\,\tilde{\sigma}_2)$ from $\tilde{\sigma}_0^2 = \langle\tilde{\Delta}^2\rangle$, $\tilde{\sigma}_1^2 = \langle(\nabla\tilde{\Delta})^2\rangle$, and $\tilde{\sigma}_2^2 = \langle(\nabla^2\tilde{\Delta})^2\rangle$. We will therefore have to treat γ_* as a free parameter in performing the fitting between theoretical predictions (16) and numerical results for the functions $F_X(\nu_t)$, $F_Y(\nu_t)$, and $F_Z(\nu_t)$ in order to determine σ_κ. We have then confirmed that γ_* is well constrained mainly by $F_X(\nu_t)$.

2.3. *Effect of Filtering*

We so far have ignored the effects of filtering. Actual CMB temperature maps will be observed with a finite angular resolution, or the artificial filtering method might be used to reduce the detector noise effect (Barreiro et al. 1998). The measured temperature map is then given by

$$\Delta^{\mathscr{F}}(\boldsymbol{\theta};\theta_s) = \int d^2\boldsymbol{\theta}'\,W(|\boldsymbol{\theta}-\boldsymbol{\theta}'|;\theta_s)\Delta(\boldsymbol{\theta}')\,, \tag{17}$$

where $W(\theta;\theta_s)$ is a window function, and throughout this paper we adopt the Gaussian beam approximation expressed by $W(\theta;\theta_s) = \exp[-\theta^2/(2\theta_s^2)]/(2\pi\theta_s^2)$. For the filtering of a telescope, the smoothing angle θ_s can be expressed in terms of its FWHM angle $\theta_{\rm FWHM}$ as $\theta_s = \theta_{\rm FWHM}/(8\ln 2)^{1/2}$. The filtered lensed temperature field is given by

$$\tilde{\Delta}^{\mathscr{F}}(\boldsymbol{\theta}) = \int d^2\boldsymbol{\theta}'\,W(|\boldsymbol{\theta}-\boldsymbol{\theta}'|;\theta_s)\Delta[\boldsymbol{\theta}'+\boldsymbol{\xi}(\boldsymbol{\theta}')]\,. \tag{18}$$

Similarly, the filtered second-derivative fields of the CMB can be expressed as

$$\begin{aligned}\tilde{\Delta}_{ij}^{\mathscr{F}}(\boldsymbol{\theta}) &= \int d^2\boldsymbol{\theta}'\,W(|\boldsymbol{\theta}-\boldsymbol{\theta}'|;\theta_s)\mathscr{A}_{im}(\boldsymbol{\theta}')\Delta_{mn} \\ &\quad\times[\boldsymbol{\theta}'+\boldsymbol{\xi}(\boldsymbol{\theta}')]\mathscr{A}_{nj}(\boldsymbol{\theta}') \\ &= \int d^2\boldsymbol{\theta}'\,W(|\boldsymbol{\theta}-\boldsymbol{\theta}'|;\theta_s) \\ &\quad\times[\Delta_{ij}(\boldsymbol{\theta}')+\Delta_{in}(\boldsymbol{\theta}')\xi_{n,j}(\boldsymbol{\theta}')+\cdots] \\ &= \int \frac{d^2\boldsymbol{l}}{(2\pi)^2}\,W(\boldsymbol{l};\theta_s)\Delta_{ij}(\boldsymbol{l})e^{i\boldsymbol{l}\cdot\boldsymbol{\theta}} \\ &\quad+\int\frac{d^2\boldsymbol{l}}{(2\pi)^2}\frac{d^2\boldsymbol{l}'}{(2\pi)^2} \\ &\quad\times W(|\boldsymbol{l}+\boldsymbol{l}'|;\theta_s)\Delta_{in}(\boldsymbol{l})\xi_{n,j}(\boldsymbol{l}') \\ &\quad\times e^{i(\boldsymbol{l}+\boldsymbol{l}')\cdot\boldsymbol{\theta}}+\cdots\,,\end{aligned} \tag{19}$$

where in the first line of right-hand side we have used the part integration and assumed that the surface integral is equal to zero for a large CMB survey sky. These equations (18) and (19) mean that the filtering procedure and the lensing effect on the CMB do not commute in a general case. Especially, the last line on the right-hand side of equation (19) shows that the information about a certain mode $\boldsymbol{l}'$ of the lensing field ξ is coupled to sidebands of the different $\boldsymbol{l}$ modes of the CMB field. The problem of mode coupling therefore has to be carefully investigated for accurate measurements of our method. However, since intrinsic CMB anisotropies have a small scale cutoff due to Silk damping and the directions of the CMB curvature and the lensing deformation field are statistically uncorrelated, we could employ a simple approximation that the filter function W in equation (19) is applied both to the CMB intrinsic field and the lensing field independently. The variance of the convergence field in equations (16) can be then expressed by

$$\sigma_\kappa^2(\theta_s) = \int \frac{d^2\boldsymbol{l}}{(2\pi)^2}\,W^2(l;\theta_s)P_\kappa(l)\,, \tag{20}$$

where $W(l;\theta_s) = \exp(-l^2\theta_s^2/2)$. Unfortunately, this approximation (20) might not be so accurate since the numerical experiments showed that the magnitude of the convergence field reconstructed by the non-Gaussian signatures in the simulated maps is smaller than the value of σ_κ computed by equation (20). Therefore, the validity or improvement of this approximation should be further investigated using numerical experiments.

3. MODELS AND NUMERICAL EXPERIMENTS

3.1. *Cosmological Models*

To make quantitative investigations, we consider some specific cosmological models. For this purpose, we adopt the currently favored flat universe in the adiabatic cold dark matter (CDM) model, where the background cosmological parameters are chosen as $\Omega_{m0} = 0.3$, $\Omega_{\lambda 0} = 0.7$, and $h = 0.7$. The flat universe is strongly supported by the recent high-precision measurements of C_l (de Bernardis et al. 2000; Hanany et al. 2000). The baryon density is chosen to satisfy $\Omega_{b0}\,h^2 = 0.019$, which is consistent with values obtained from the measurements of the primeval deuterium abundance (Burles & Tytler 1998). To compute C_l used to make realizations of numerically simulated CMB maps, we used

the helpful CMBFAST code developed by Seljak & Zaldarriaga (1996). As for the matter power spectrum used to compute lensing contributions to both numerical and theoretical predictions, we employed the Harrison-Zeldovich spectrum and the BBKS transfer function with the shape parameter from Sugiyama (1995). The free parameter is only the normalization of the present-day matter power spectrum, i.e., σ_8. The nonlinear evolution of the power spectrum is modeled using the fitting formula given by Peacock & Dodds (1996).

3.2. *Numerical Simulations of the CMB Maps with and without Lensing*

We perform numerical simulations of the CMB maps with and without the lensing effect following the procedure presented in Takada & Futamase (2001) in detail. First, a realistic temperature map on a fixed square grid can be generated from a given power spectrum, C_l, based on the Gaussian assumption. Each map is initially $60^\circ \times 60^\circ$ area, with a pixel size of about $0\farcm88$ ($=60^\circ/4096$). A two-dimensional lensing displacement field can be also generated as a realization of a Gaussian process using the power spectrum of the convergence field, P_κ, defined by equation (11). Note that we have now employed a technical simplification that the displacement field is assumed to be Gaussian. As explained, the lensing effect is then computed as a mapping between the observed and primordial temperature field expressed by $\tilde{\Delta}(\boldsymbol{\theta}) = \Delta(\boldsymbol{\theta} + \boldsymbol{\xi})$. The temperature field on a regular grid in the lensed map is then given by a primordial field on a irregular grid using a simple local linear interpolation of the temperature field in the neighbors (the so-called could-in-cell interpolation). In the case of taking into account the instrumental effects of beam smearing and detector noise, we furthermore smooth out the temperature map by convolving the Gaussian window function and then add randomly the noise field into each pixel.

Figure 2 shows an example of simulated unlensed (*left*) and lensed (*right*) CMB maps, where the isotemperature contours are also drawn in steps of $\Delta\nu_t = 0.2$. This figure illustrates that the regions around crowded contours with a higher absolute temperature threshold and larger curvatures are more strongly deformed by the lensing. Previous works (Seljak & Zaldarriaga 2000; Zaldarriaga 2000) have pointed out another but partly similar feature that the power of anisotropies on small scales generated by the lensing is correlated with the larger scale gradient of the intrinsic CMB field.

3.3. *The CMB Curvature Field*

To calculate the second-derivative fields of the CMB at a certain pixel in the simulated maps, we used a method of finite differences between neighboring pixels around the point:

$$\Delta_{11}(i, j) = [\Delta(i - 1, j + 1) - 2\Delta(i, j) + \Delta(i + 1, j)]/\delta x^2 ,$$

$$\Delta_{12}(i, j) = \frac{1}{4\delta x^2} [\Delta(i - 1, j - 1) - \Delta(i - 1, j + 1) - \Delta(i + 1, j - 1) + \Delta(i + 1, j + 1)] , \quad (21)$$

where δx is the pixel size and $\Delta(i, j)$ is the local temperature fluctuations at the grid point (i, j).

4. RESULTS AND COSMOLOGICAL IMPLICATIONS

4.1. *Numerical Results*

In Figure 3, we show the numerical results of the lensed or unlensed three functions (16) with respect to the temperature threshold ν_t, which are obtained from each of 150 realizations of the CMB maps with $60^\circ \times 60^\circ$ area for the filter scale of $3'$. All the curves are plotted at intervals of $\Delta\nu_t = 0.1$. The error bar in each bin corresponds to the cosmic variance associated with the measurements and is estimated by rescaling the variances obtained from all the realizations by a factor of $\frac{1}{8}$ when we assume a sky coverage

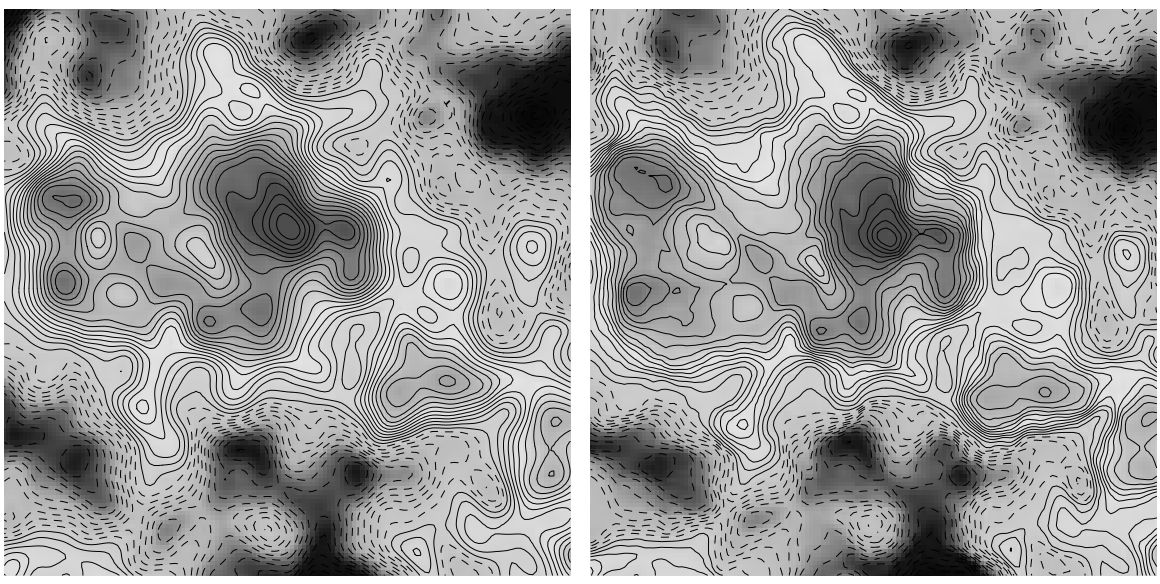

FIG. 2.—Examples of simulated primordial CMB anisotropies map (*left*) and lensed map (*right*). We here adopted the adiabatic CDM flat universe model with $\Omega_{m0} = 0.3$, $\Omega_{\lambda 0} = 0.7$, and $h = 0.7$. The figures are on a side of 2° and the isotemperature contours are drawn in intervals of $\Delta\nu_t = 0.2$ [$\nu_t \equiv \Delta(\boldsymbol{\theta})/\sigma_0$].

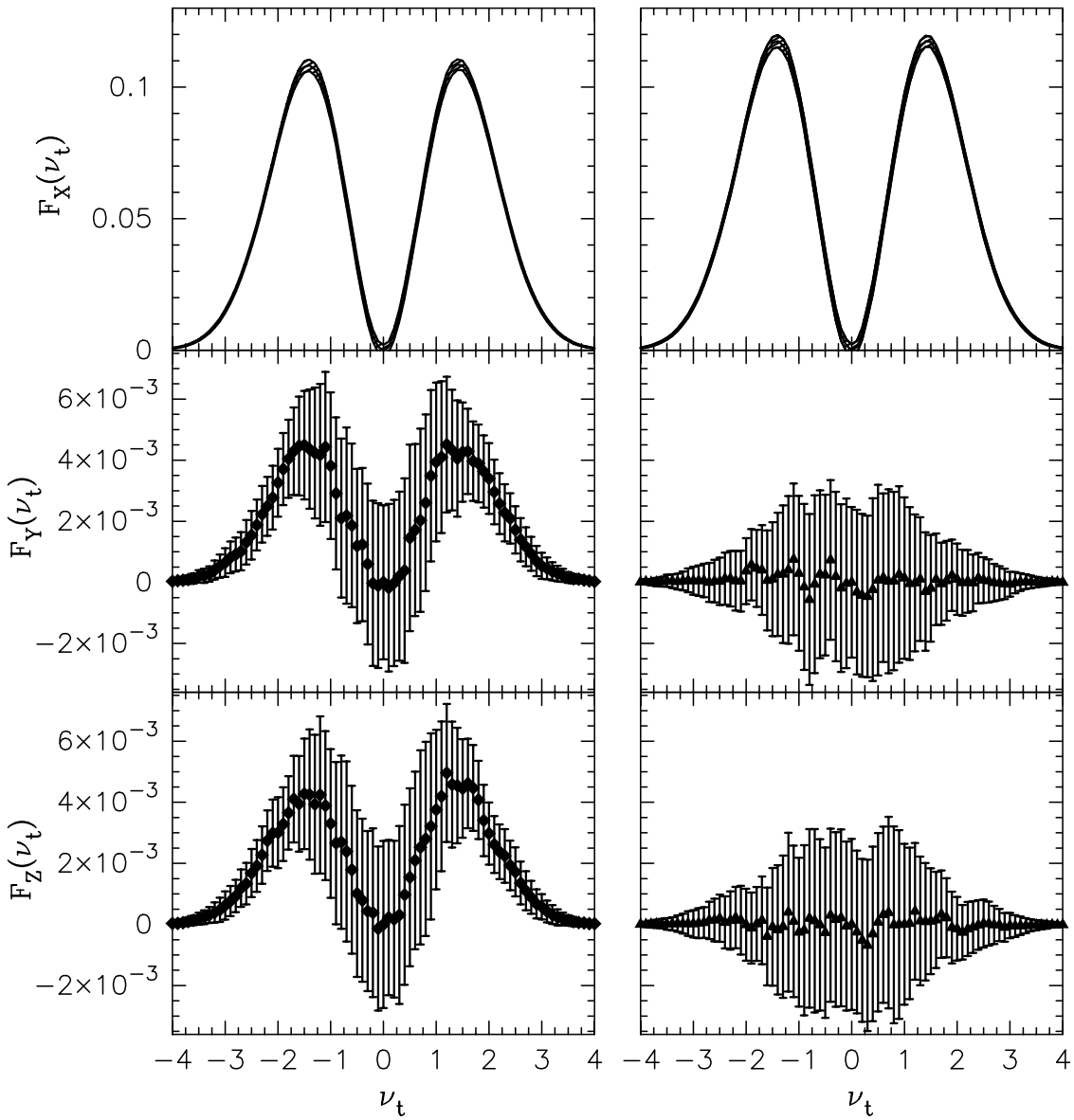

FIG. 3.—Lensed (*left*) and unlensed (*right*) shapes of three functions (16) of the isotemperature statistics with a filter scale of 3′ and $\sigma_8 = 2.0$ with respect to the temperature threshold ν_t, which are computed using the numerical simulations of CMB maps. The background cosmological parameters are $\Omega_m = 0.3$, $\Omega_{\lambda 0} = 0.7$, and $h = 0.7$. The triangular and round marks in each panel correspond to the averages obtained from each of 150 independent realizations of the unlensed and lensed maps, respectively. The error bars denote 1 σ errors due to cosmic variance computed for 70% sky coverage of a CMB survey. The lensed curves $F_Y(\nu_t)$ and $F_Z(\nu_t)$ clearly show that lensing generates a significant functional dependence on ν_t approximately expressed by the form $\propto \nu_t^2 \exp(-\nu_t^2/2)$, whereas the unlensed shapes have random errors with both positive and negative values around $F_Y(\nu_t) = F_Z(\nu_t) = 0$ in each bin of ν_t.

of 70% ($f_{\rm sky} = 0.7$) for a survey of the CMB sky. The figure clearly shows that the lensing deformation effect generates a significant functional dependence on ν_t of $F_Y(\nu_t)$ and $F_Z(\nu_t)$ approximately expressed in the form proportional to $\nu_t^2 \exp(-\nu_t^2/2)$. Especially, the non-Gaussian signatures are pronounced at high absolute thresholds such as $|\nu_t| \gtrsim 1$ as a result of the strong coupling between the gravitational tidal shear and the large CMB curvature at such high thresholds, as explained. For a Gaussian case, $F_Y(\nu_t)$ and $F_Z(\nu_t)$ should be equal to zero at all bins of ν_t and thus have both positive and negative large values of the cosmic variance in each bin, although the mean values do not exactly converge to zero yet for the number of our realizations. These results therefore mean that the non-Gaussian signatures induced by lensing could be significantly distinguished compared to cosmic variance. In Figure 4 we show the contour map of $\langle (F_{Xi} - \langle F_{Xi}\rangle)(F_{Xj} - \langle F_{Xj}\rangle)\rangle/(\sigma_i \sigma_j)$ calculated from those realizations, where $\langle F_{Xi}\rangle$ is the mean value and σ_i the variance of the estimators of $F_X(\nu_t)$ at threshold bin ν_i. We have confirmed that the correlations for $F_Y(\nu_t)$ and $F_Z(\nu_t)$ are similar to the result in this figure. These correlations would be required in order properly to quantify the significance of any departure from Gaussian statistics when performing the fitting between the numerical results and theoretical predictions. Figure 4 indicates and we have actually confirmed that, if we take the data at intervals of $\Delta\nu_t \approx 0.5$, the correlation matrix comes to be very close to diagonal in each bin for all the cases that we consider in this paper. Taking into account this result, the following results are shown in intervals of $\Delta\nu_t = 0.5$.

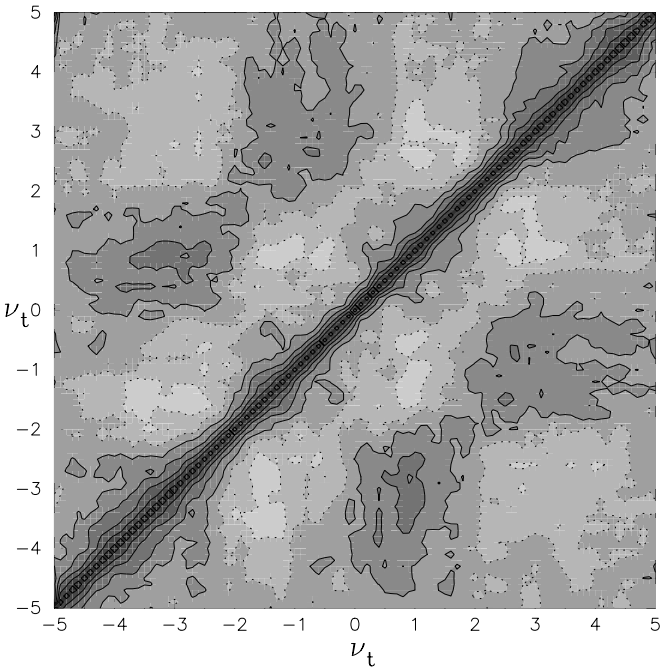

FIG. 4.—Contours of correlation coefficients, $\langle (F_{Xi} - \langle F_{Xi} \rangle)(F_{Xj} - \langle F_{Xj} \rangle) \rangle / (\sigma_i \sigma_j)$, for estimators of the function $F_X(\nu_t)$ defined by eq. (16). Here F_{Xi} and σ_i denote the values and variance computed from the simulated CMB map in the threshold bin ν_{ti}. The contour is stepped in units of 0.2, and the solid and dotted contours denote positive and negative values of the coefficients.

Figure 5 demonstrates the results with the filtering scale of 5′.5 computed similarly as in Figure 3. One can see that increasing the filtering scale decreases the magnitude of lensing signals for $F_Y(\nu_t)$ and $F_Z(\nu_t)$, because the filtering again tends to circularize the deformed structures in the CMB map as pointed out by Bernardeau (1998). However, even in this case of $\theta_{\rm FWHM} = 5'.5$, the lensed curves $F_Y(\nu_t)$ and $F_Z(\nu_t)$ remain having the distinct functional dependence on ν_t compared to the Gaussian case of $F_Y(\nu_t) = F_Z(\nu_t) = 0$. In practice, it is important to also take into account the detector noise effect on our method. We here assume the instrumental specification of the 217 GHz channel of the satellite mission *Planck Surveyor*: the noise level of $\sigma_N = 4.3 \times 10^{-6}$ pixel^{-1} on a side of the FWHM extent ($\theta_{\rm FWHM} = 5'.5$). The noise field at the original fine grid is also convolved with the Gaussian filter of FWHM scale to avoid domination of noise spikes at small angular scales (Barreiro et al. 1998). Figure 6 shows the results. The noise effect reduces the amplitudes of $F_X(\nu_t)$ compared to those in Figure 5 as a result of the change of quantity $\gamma_* \ (\equiv \sigma_1^2/\sigma_0\sigma_2)$ for intrinsic CMB anisotropies due to the noise. Even in this case, the figure clearly shows that the noise level of *Planck* does not largely change the lensed shapes of F_Y and F_Z compared to the results of Figure 5, although the lensing signals at low thresholds such as $|\nu_t| \lesssim 1.5$ are weakened. Importantly, significant non-Gaussian signatures on $F_Y(\nu_t)$ and $F_Z(\nu_t)$ still remain compared to $F_Y(\nu_t) = F_Z(\nu_t) = 0$. This is because our method has so far relied on the normalized observable quantities such as $\nu(\theta) = \Delta(\theta)/\sigma_0$ and those quantities are more robust against the systematic contributions of the detector noise than the CMB fields themselves, which are certainly affected by the noise. Figure 7 shows the results with $\sigma_8 = 2.5$ similarly as Figure 6. This figure explains that the lensing signals can significantly deviate from the unlensed case if the lensing effect is adequately large.

4.2. *Cosmological Implications from the Lensing-induced Non-Gaussian Signatures*

Another important question that we should address is how useful cosmological information on large-scale structure formation can be extracted from the lensing signals onto the isotemperature statistics presented in the previous subsection. Since equation (16) shows that the non-Gaussian signatures depend on γ_* and σ_κ, we come to consider the problem of how accurately the contribution of σ_κ can be determined. As shown by Jain & Seljak (1997), the magnitude of σ_κ is sensitive to the σ_8 and Ω_{m0} parameters for the CDM models and also depends on the filtering scale θ_s for a realistic case. From equation (20) we find that σ_κ thus has the following approximate scaling relations for flat universe models around the fiducial model ($\Omega_{m0} = 0.3$, $\Omega_{\lambda 0} = 0.7$, and $h = 0.7$):

$$\sigma_\kappa(3') \approx 0.157(\theta_{\rm FWHM}/3')^{-0.35}(\sigma_8/2.0)^{1.1} \times (\Omega_{m0}/0.3)^{0.25} ,$$
$$\sigma_\kappa(10') \approx 9.67 \times 10^{-2}(\theta_{\rm FWHM}/10')^{-0.47} \times (\sigma_8/2.0)^{1.0}(\Omega_{m0}/0.3)^{0.10} . \quad (22)$$

Furthermore, since more fundamental information is contained in the three-dimensional mass fluctuations, we have to take into account the projection effect (Jain & Seljak 1997; Seljak & Zaldarriaga 1999; Zaldarriaga & Seljak 1999; Takada & Futamase 2001). The convergence field at $\theta \lesssim 10'$ depends mainly on mass fluctuations with wavelength modes of $\lambda \lesssim 10\,h^{-1}$ Mpc and structures distributed in wide redshift ranges of $0 \lesssim z \lesssim 10$ peaked at $z \approx 3$. The lensing distortion effect on the CMB map can thus be a powerful probe of large-scale structures up to high redshift in principle, which is not attainable by any other means.

Table 1 summarizes the results obtained for the determination of σ_κ with a best fit and 1 σ error, which arises from cosmic variance or also includes errors due to the detector noise effect. The "analytic" value of σ_κ in this table is calculated using the approximation for the beam smearing given by equation (20). We here performed χ^2 fitting between the numerical results and theoretical predictions for $F_X(\nu_t)$, $F_Y(\nu_t)$, and $F_Z(\nu_t)$. Note that we have used all data of the functions in the range $-4 \le \nu_t \le 4$ at intervals of $\Delta\nu_t = 0.5$, because the correlation matrix for those data is close to diagonal, as explained in Figure 4. Thus, the theoretical predictions of $F_X(\nu_t)$, $F_Y(\nu_t)$, and $F_Z(\nu_t)$ are given by the two free parameters γ_* and σ_κ expressed by equation (16). Most importantly, Table 1 clearly shows that σ_κ estimated from the non-Gaussian signatures on F_X, F_Y, and F_Z could be significantly detected with high signal-to-noise ratios compared to the unlensed case. Here, the 1 σ error for the σ_κ determination corresponds to $\Delta\chi^2 = 2.3$ for the χ^2 fitting. Figure 8 demonstrates an example of the best-fit results for the noise case with $\sigma_8 = 2.0$ and $\theta_{\rm FWHM} = 5'.5$. This figure shows that σ_κ is constrained mainly from the numerical data of $F_Y(\nu_t)$ and $F_Z(\nu_t)$ at $|\nu_t| \gtrsim 2$ that have relatively small cosmic variances. On the other hand, γ_* is well constrained only by the data of $F_X(\nu_t)$. Even if we use the value of $\tilde{\gamma}_*$ directly measured from the lensed simulated CMB

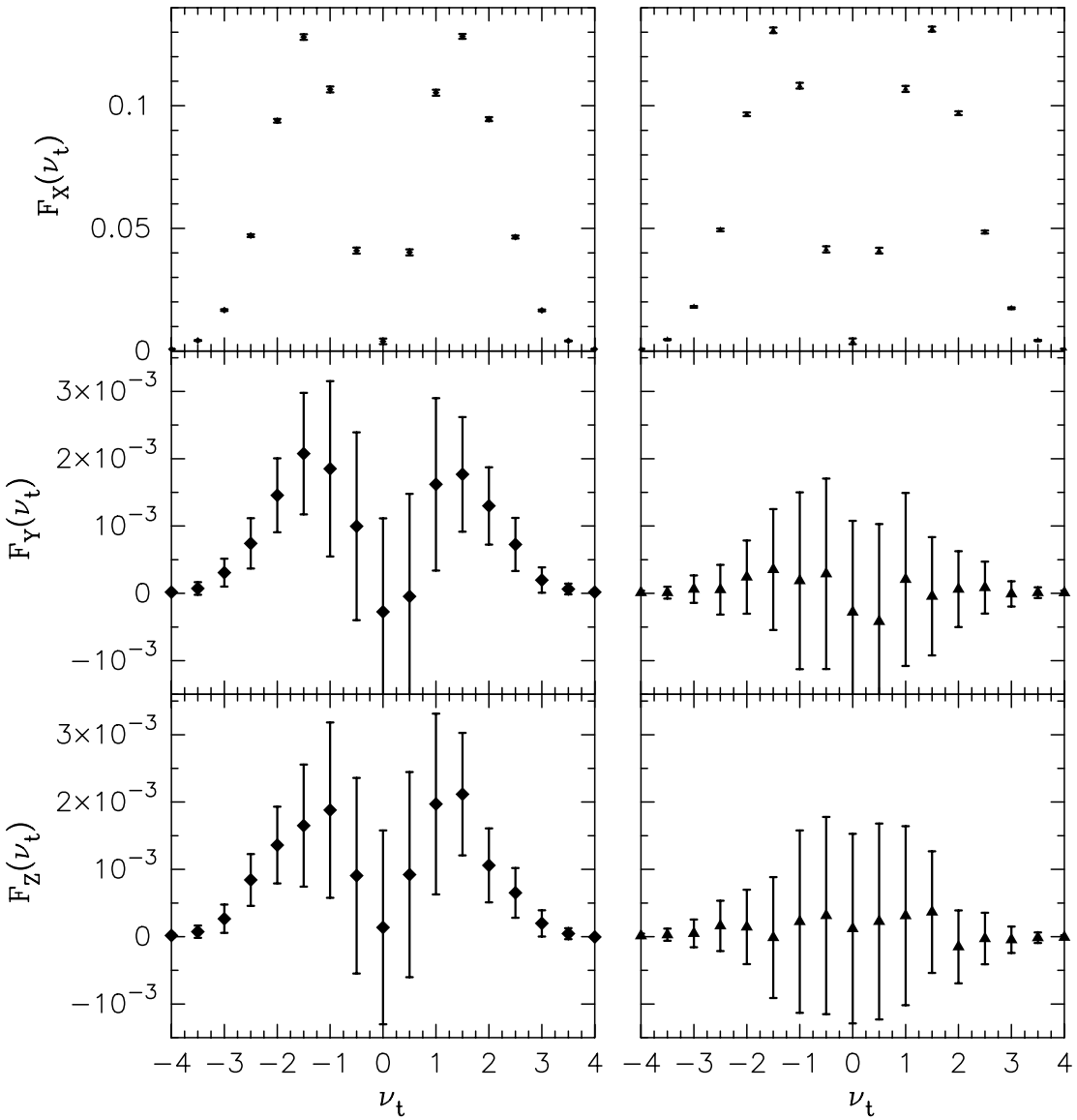

FIG. 5.—Same as Fig. 3, with a 5′.5 filtering scale and $\sigma_8 = 2.0$. All the plots are shown in intervals of $\Delta\nu_t = 0.5$, taking into account the result of Fig. 4.

TABLE 1

VALUES OF σ_κ FROM BEST-FIT PARAMETERIZATIONS

σ_8	Filter Scale (arcmin)	Analytic $\sigma_\kappa^2 \times 10^2$	$\sigma_\kappa^2 \times 10^2$, Best Fit
0.0 (no lens).....	3	...	0.02 ± 0.03
0.0 (no lens).....	5.5	...	0.04 ± 0.03
0.0 (no lens).....	5.5 + noise	...	0.03 ± 0.04
1.5	3	1.31	0.71 ± 0.04
1.5	5.5	0.86	0.26 ± 0.03
1.5	5.5 + noise	0.86	0.23 ± 0.04
2.0	3	2.47	1.14 ± 0.04
2.0	5.5	1.57	0.42 ± 0.04
2.0	5.5 + noise	1.57	0.41 ± 0.05
2.0	8	1.15	0.07 ± 0.04
2.5	5.5	2.51	0.62 ± 0.04
2.5	5.5 + noise	2.51	0.56 ± 0.05

NOTES.—Errors give the cosmic variance (or also include the instrumental errors caused by detector noise) for a 70% sky coverage survey of the CMB map. Here, the analytic value of σ_κ is calculated by the approximation (20) for the beam-smearing effect.

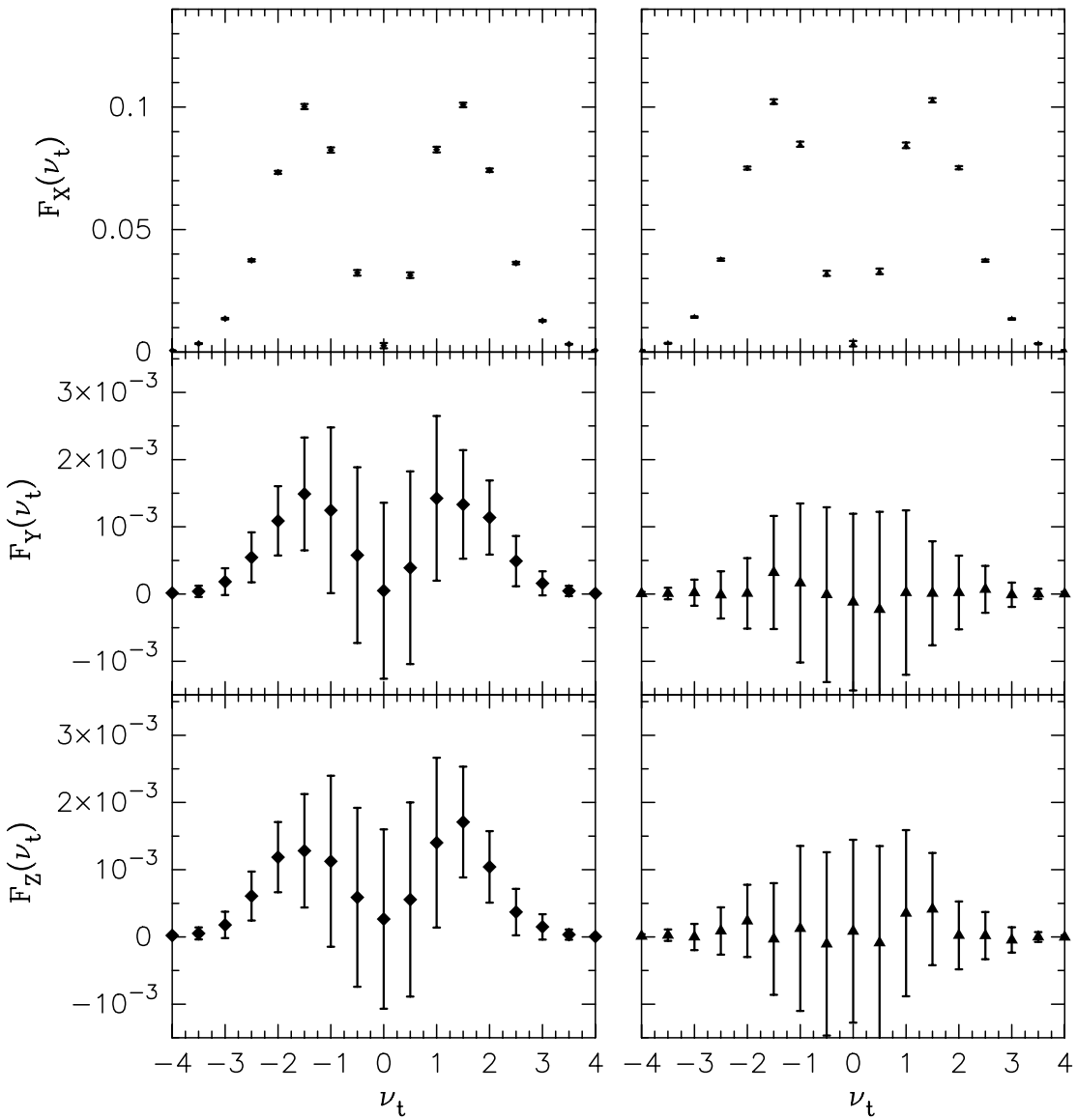

FIG. 6.—This figure includes the detector noise effect for the case shown in Fig. 5, where we have assumed the noise level of *Planck* expressed in terms of the variance of noise field per 5.5 FWHM pixel as $\sigma_{\rm pix} = 4.3 \times 10^{-6}$. Note that the scales of the x- and y-axes are the same as in Fig. 5.

maps instead of the fitting parameter γ_* (see the paragraph under eq. [16]), it causes only the slight change of results in Table 1. One might then consider a possibility to determine σ_κ by comparing the measured $\tilde{\gamma}_*$ from the CMB maps to that of γ_* obtained from the fitting of $F_X(\nu_t)$ through the relation of $\tilde{\gamma}_* = \gamma_*(1 - 7\sigma_\kappa^2/2)$, but the constraint is much weaker than that of using the non-Gaussian signatures on $F_Y(\nu_t)$ and $F_Z(\nu_t)$. Table 1 also shows that the beam-smearing effect is crucial for our method and, in the case with $\theta_{\rm FWHM} = 8'$ and $\sigma_8 = 2.0$, the lensing signatures are obscured by the cosmic variance. On the other hand, the detector noise effect does not largely affect the results. However, we have to note that the best-fit value of σ_κ in all the considered cases is underestimated compared to the analytic value of σ_κ calculated by approximation (20) for the beam-smearing effect. The possible reasons for the underestimation are ascribed to the effect of the discrete pixel in the simulated maps or to the mode coupling between the CMB field and lensing field caused by the filtering, as explained in § 2.3. So far, it is concluded based on the following results that the reason is mainly due to the discrete pixel effect. We have confirmed that the best-fit value of γ_* even for the unlensed case by our method also underestimates the value of γ_* calculated by the conventionally used approximation (e.g., Bond & Efstathiou 1987) expressed in terms of C_l and $\theta_{\rm FWHM}$ as $\gamma_* \equiv \sigma_1^2(\theta_{\rm FWHM})/\sigma_0(\theta_{\rm FWHM})\sigma_1(\theta_{\rm FWHM})$, where $\sigma_i^2(\theta_{\rm FWHM}) \equiv \int (l\,dl/2\pi) l^{2i} C_l \exp(-l^2\theta_s^2)$ in the context of the small-angle approximation and $\theta_s = \theta_{\rm FWHM}/(8\ln 2)^{1/2}$. For example, values of the best fit and analytical prediction for γ_* are 0.368 and 0.38, respectively, for the unlensed case with $\theta_{\rm FWHM} = 5.5$ and without the detector noise effect. For the discrete pixel data of simulated CMB maps, it is generally difficult to perform accurate measurements of statistical quantities defined from any *derivative* fields of the CMB compared with their analytical predictions. Schmalzing et al. (2000) have also confirmed that it is crucial for accurate measurements of Minkowski functionals in a realistic CMB

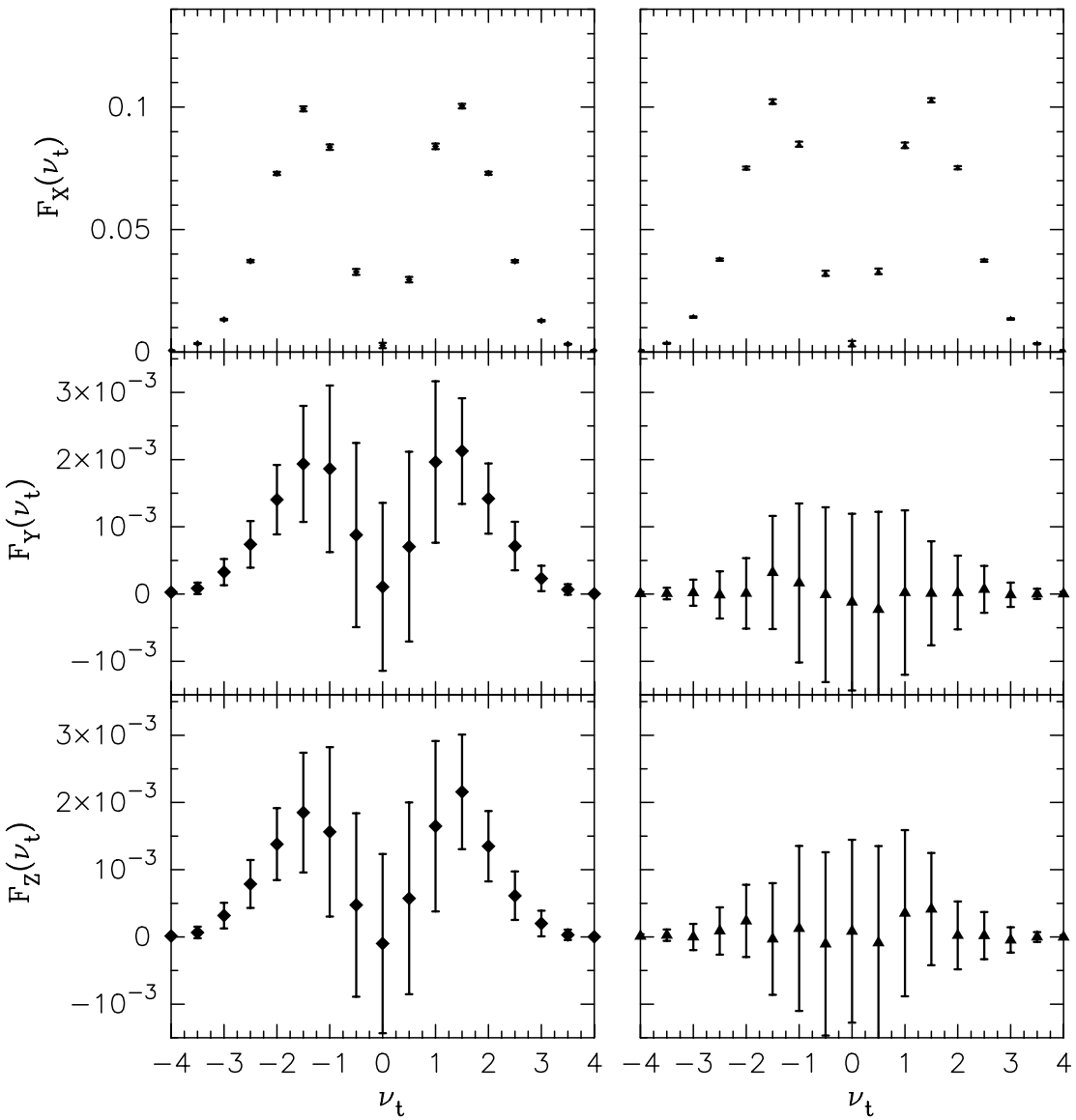

FIG. 7.—Same as Fig. 6, with $\sigma_8 = 2.5$

map to take into account the effect of discrete pixels, where we have used the interpolation technique. Therefore, we have to further investigate the problem of how the σ_κ determination from a realistic CMB map performed by our method can reproduce its simple analytic prediction, for example, by using the numerical simulations combined with the interpolation technique.

5. DISCUSSION AND CONCLUSION

In this paper, we developed a new simple method for extracting lensing-induced non-Gaussian signatures on isotemperature statistics in the CMB sky and also investigated the feasibility of method using numerical experiments. Importantly, by focusing on the characteristic three independent functions obtained from the averages of quadratic combinations of the second derivatives of the CMB field over the isotemperature contours with each temperature threshold, it was found that weak lensing generates non-Gaussian signatures on those functions that have a distinct functional dependence on the threshold. The result is a consequence of the coupling between the gravitational tidal shear and the CMB curvature [defined by $-(\Delta_{11} + \Delta_{22})/\sigma_2$] through the intrinsic correlation between the CMB curvature and the temperature threshold predicted by the Gaussian theory. By means of the non-Gaussian signatures, it can be expected that the lensing signals are extracted from the observed CMB data irrespective of the C_l measurements, or equivalently, the assumptions for the fundamental cosmological parameters. Our numerical experiments indeed showed that the method allows us to extract the lensing signals with a high signal-to-noise ratio, provided that we have CMB maps with sufficiently low noise and high angular resolution as given by the *Planck* mission. Recently, Seljak & Zaldarriaga (1999; see also Zaldarriaga & Seljak 1999) developed a powerful method for a direct reconstruction of the projected power spectrum of matter fluctuations from the lensing deformation effect on the CMB maps. The method focuses on the averages of quadratic combinations of the gradient fields of the CMB over a lot of independent patches in the CMB sky, like the analysis of the measurements of the coherent gravitational distortion on images of distant galaxies due to

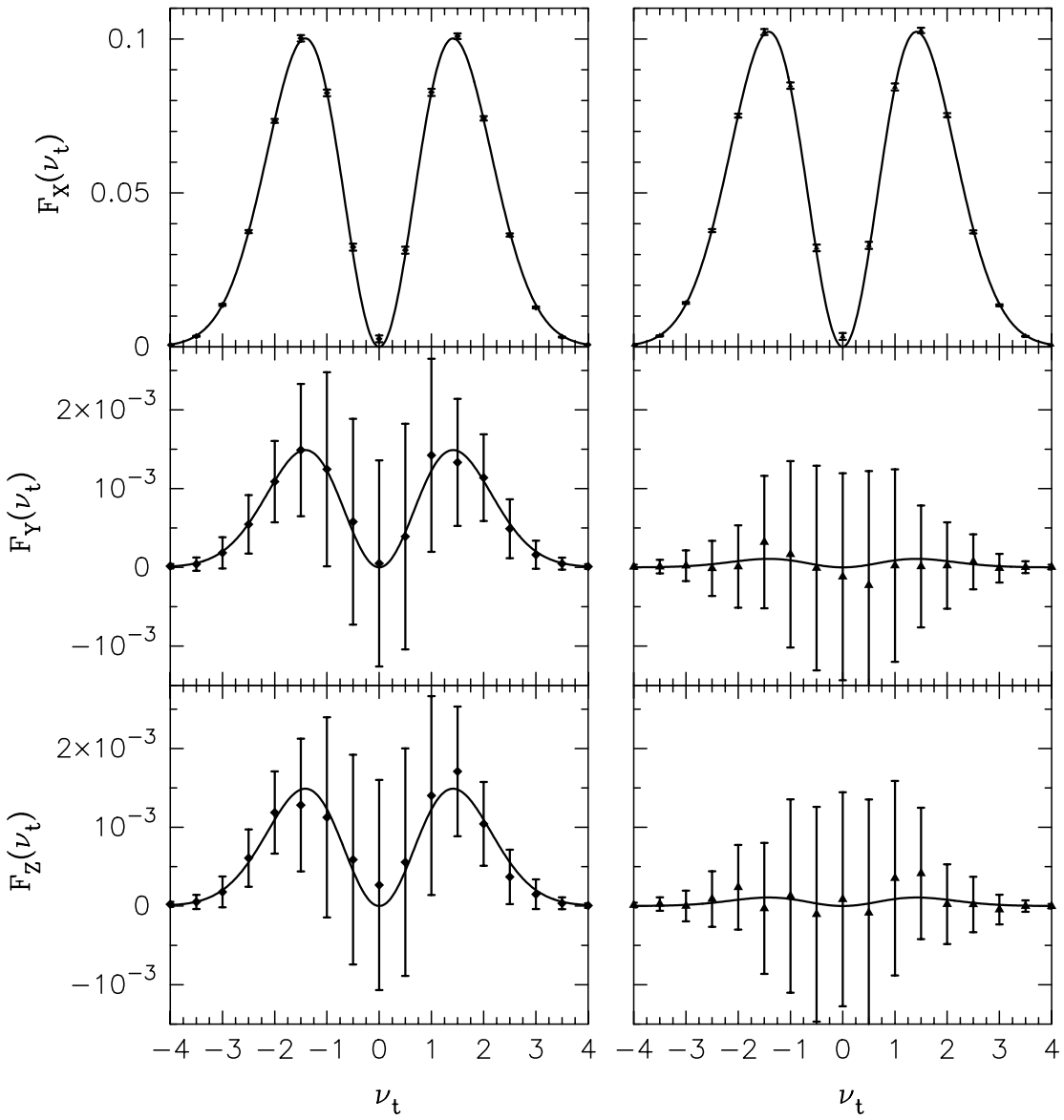

FIG. 8.—Results of the best fit between the theoretical predictions and the numerical results for the lensed (*left*; $\sigma_8 = 2.0$) and unlensed (*right*) cases with $\theta_{\rm FWHM} = 5'.5$ and the noise effect. The line in each panel shows the best-fit theoretical prediction (16) (see Table 1).

large-scale structure. In this method, the lensing signatures on individual patches are extracted as differences between the measured statistical measures and their all-sky averages. They showed that the reconstruction of the input projected matter power spectrum could be successfully achieved if there is no sufficient small-scale power of intrinsic CMB anisotropies. In this sense, however, the method partly depends on the statistical measurements of intrinsic CMB anisotropies, and this is the main difference between their and our method that we would like to stress. Moreover, our method focuses on the second-derivative fields of the CMB and, therefore, is more sensitive to the amplitudes of the projected matter power spectrum on smaller angular scales. Anyway, since the lensing signals in the observed CMB sky are weak, we think that some independent statistical methods should be performed to extract them, which could also lead to constraints on the projected matter power spectrum at respective, different angular scales.

Extending our method presented in this paper, one might consider a following possibility to extract the lensing distortion effect. BBKS and BE have shown that structures around local higher maxima or lower minima of temperature fluctuation fields tend to have a more peaked shape and be more spherically symmetric around the peaks in the Gaussian (unlensed) case. From these features, it can also be expected that weak lensing causes stronger distortion effects on structures around the higher maxima (or lower minima) and might provide us more significant non-Gaussian signatures as a function of the temperature threshold of peaks than our method did. However, as quantitatively shown by Bernardeau (1998), the statistical measure for the peaks provides the same or lower signal-to-noise ratio as or than the statistics for a field point taking into account cosmic variance, where he investigated the lensing effect on the probability distribution function of ellipticities around field points or peaks. This is because the number density of peaks in the CMB sky is not so sufficient for these statistical measurements. For this reason, we foresee a similar conclusion for the signal-to-noise ratio obtained from the measurements of the lensing distortion

effect on the structures around peaks using our method, although this work will have to be further investigated carefully.

Recently, Schmalzing et al. (2000) have shown that the lensing effect on the Minkowski functionals (the morphological descriptions of the CMB map) appears just as a change of their normalization factors against the Gaussian predictions using numerical experiments. We indeed have confirmed that the analytical predictions for the lensed Minkowski functionals done in a similar way as presented in this paper give the same conclusion as the numerical results. The result comes from the fact that the lensing does not largely change the global topology of CMB anisotropies in a statistical sense. Likewise, it is known that the gravitational potential from which the shear is generated is invariant under the parity transformation and lensing does not induce the so-called B-type polarization defined from combinations of the derivative fields of CMB fluctuations (Seljak & Zaldarriaga 1999; Zaldarriaga & Seljak 1999). These results mean that weak lensing cannot simply generate a new mode of pattern of the CMB anisotropies that is absent in the Gaussian case. For these reasons, in this paper we focus on other information on statistical properties of the intrinsic CMB that is useful for the study of lensing effects and can be specifically predicted based on Gaussian random theory. Another issue that we should discuss is the possible effect on our results caused by non-Gaussian features on the convergence field of the large-scale structure at $\theta < 10'$ that is revealed by ray-tracing simulations (Jain et al. 2000; Hamana et al. 2000), which we have ignored in the numerical experiments of the lensed CMB maps. However, since the lensing effect on the CMB can be treated as a mapping, which is expressed as $\tilde{\Delta}(\boldsymbol{\theta}) = \Delta(\boldsymbol{\theta} + \boldsymbol{\xi})$, and the lensing contributions to the CMB are always coupled to the contributions from the primary CMB fields, we foresee that the effect will not change the functional dependence on the temperature threshold of the lensing-induced non-Gaussian signatures of $F_X(\nu_t)$, $F_Y(\nu_t)$, and $F_Z(\nu_t)$ expressed by equation (16), even if the effect could enhance the magnitudes.

Undoubtedly, other secondary effects could induce non-Gaussian properties in the observed CMB map. The most important effects are the (thermal) Sunyaev-Zeldovich effect and the foreground contaminations such as Galactic foreground and extragalactic point sources. Those effects can be removed to some extent by using advantages of their spectral properties, although further reliable investigations should be done for any measurements of the CMB. Furthermore, in this paper we have presented the lensing-induced non-Gaussian signatures on *three* independent functions, $F_X(\nu_t)$, $F_Y(\nu_t)$, and $F_Z(\nu_t)$, and therefore we expect that the property $F_Y(\nu_t) = F_Z(\nu_t)$ can provide us a clue to resolving the lensing contributions from the other secondary effects.

The author would like to thank T. Futamase and J. Schmalzing for fruitful discussions and valuable comments. He also acknowledges the useful comments from the anonymous referee. He thanks U. Seljak and M. Zaldarriaga for making their CMBFAST code publicly available. He also acknowledges support from a Japan Society for Promotion of Science (JSPS) Research Fellowship.

REFERENCES

Bacon, D., Refregier, A., & Ellis, R. 2000, MNRAS, 318, 625
Balbi, A., et al. 2000, ApJ, 545, L1
Bardeen, J. M., Bond, J. R., Kaiser, N., & Szalay, A. S. 1986, ApJ, 304, 15 (BBKS)
Barreiro, R. B., Sanz, J. L., Martínez-González, E., & Silk, J. 1998, MNRAS, 296, 693
Bernardeau, F. 1998, A&A, 338, 767
Blandford, R. D., Saust, R. D., Brainerd, A. B., & Villumsen, J. V. 1991, MNRAS, 251, 600
Bond, J. R., & Efstathiou, G. P. 1987, MNRAS, 226, 655 (BE)
Burles, S., & Tytler, D. 1998, ApJ, 507, 732
de Bernardis, P., et al. 2000, Nature, 404, 955
Gunn, J. 1967, ApJ, 147, 61
Guth, A., & Pi, S.-Y. 1982, Phys. Rev. Lett., 49, 1110
Hamana, T., Martel, H., & Futamase, T. 2000, ApJ, 529, 56
Hanany, S., et al. 2000, ApJ, 545, L5
Hu, W., Fukugita, M., Zaldarriaga, M., & Tegmark, M. 2001, ApJ, 549, 669
Hu, W., Sugiyama, N., & Silk, J. 1997, Nature, 386, 37
Jain, B., & Seljak, U. 1997, ApJ, 484, 560
Jain, B., Seljak, U., & White, S. D. M. 2000, ApJ, 530, 547
Kaiser, N. 1992, ApJ, 388, 272
Kaiser, N., Wilson, G., & Luppino, G. 2000, ApJ, submitted (astro-ph/0003338)
Lange, A. E., et al. 2001, Phys. Rev. D, 63, 042001
Maoli, R., Van Waerbeke, L., Mellier, Y., Schneider, P., Jain, B., Bernardeau, F., Erben, T., & Fort, B. 2001, A&A, 368, 766
Miralda-Escude, J. 1991, ApJ, 380, 1
Peacock, J. A., & Dodds, S. J. 1996, MNRAS, 280, L19
Schmalzing, J., Takada, M., & Futamase, T. 2000, ApJ, 544, L83
Seljak, U. 1996, ApJ, 463, 1
Seljak, U., & Zaldarriaga, M. 1996, ApJ, 469, 437
———. 1999, Phys. Rev. Lett., 82, 2636
———. 2000, ApJ, 538, 57
Sugiyama, N. 1995, ApJS, 100, 281
Takada, M., & Futamase, T. 2001, ApJ, 546, 620
Takada, M., Komatsu, E., & Futamase, T. 2000, ApJ, 533, L83
Tegmark, M., & Zaldarriaga, M. 2000, Phys. Rev. Lett., 85, 2240
Van Waerbeke, L., Bernardeau, F., & Benabed, K. 2000a, ApJ, 540, 14
Van Waerbeke, L., et al. 2000b, A&A, 358, 30
Wittman, D., Tyson, J., Kirkman, D., Dell'Antonio, I., & Bernstein, G. 2000, Nature, 405, 143
Zaldarriaga, M. 2000, Phys. Rev. D, 62, 063510
Zaldarriaga, M., & Seljak, U. 1999, Phys. Rev. D, 59, 123507